Quantal phase-space analysis of the driven surface-state electron

Mark J. Stevens and Bala Sundaram
Department of Physics and Astronomy, The Johns Hopkins University, Baltimore, Maryland 21218
(Received 2 May 1988)

The quantum-mechanical phase space of the surface-state electron is studied in the presence of a time-dependent field, for which the classical dynamics has been shown to be chaotic. A coherent-state representation of the Wigner function for the surface-state electron Hamiltonian is constructed. This is then used to compare and contrast phase-space characteristics for quantum states initially in regular and irregular regions of the classical phase space. In particular, the effects of the driving frequency on the dynamics are examined in detail. We confirm that at larger frequencies, for a fixed field strength, the quantum phase-space evolution is restricted or localized. This localization is in contrast with the diffusive behavior still present in the classical evolution. The quantal evolution, at higher frequencies, appears better characterized by tunneling rather than by diffusion.

I. INTRODUCTION

The ionization of highly excited hydrogen atoms by microwave photons has generated a great deal of interest recently.[1,2] Much of the initial impetus came from experimental studies that reported the observation of enhanced ionization rates.[1,2] The process was seen to be highly nonperturbative in nature as, at typical experimental microwave frequencies ($\cong 10$ GHz), on the order of 100 photons are required for ionization. In normal perturbation theory this would be a 100th-order process and, consequently, would not be important. The highly excited nature of the atom (principal quantum number upwards of $n=40$), however, implies that the system is not far from its classical limit. This motivated early studies to address this problem through the classical dynamics. In large part, the attention this problem has received has been provoked by the success of classical calculations in reproducing novel features in the experiments,[1] coupled with the fact that the classical dynamics, beyond a frequency and field dependent threshold, exhibit a transition from quasiperiodic to nonquasiperiodic motion.[3] The onset of nonquasiperiodic motion is seen as a precursor to ionization at thresholds lower than those predicted earlier. It is these experimental signatures that make this system an attractive candidate in the search for quantal manifestations of nonlinear classical dynamics.

Quantum calculations for this system are inherently more tedious than the classical ones. In the last few years, however, a number of such studies have been reported[2] and some insight has been gained into the origin of the enhanced ionization mechanism in terms of the quantal dynamics. Further progress has been hindered by the fact that, in the area of nonlinear analysis, classical intuition is well developed whereas (nonrelativistic) quantum mechanics is just beginning to deal with such problems. Ideally, one would like to draw correspondences between the ideas already present in classical theory with those in quantum theory. For example, surface of section plots can give detailed information about the dynamics of the system. A quantal analogue of the surface of section would provide similar information about the quantal dynamics.

In such an attempt, a function endowed with many properties of a phase-space probability distribution, introduced by Wigner,[4] has been used to study quantal phase-space structure for a variety of systems.[5–7] Much interest has been displayed in this function as in the classical limit; it reduces to the classical phase-space probability density. The body of literature in this diverse field is vast[8] and we make no attempt to do justice to it but restrict ourselves to a few relevant examples. The semiclassical limit in both regular and irregular regions of classical phase space has been addressed[5] as well as analysis of the Wigner function for the Henon-Heiles[6] and kicked rotor systems.[7] These (and other) studies concur that for some quantal states in the classically irregular region of phase space the function extends over much of the available phase space. This is in sharp contrast to its nature in the regular region.

The Wigner function possesses many properties of the classical phase-space density though there are some significant differences. One major difference is that the function is not positive definite making a direct probabilistic interpretation invalid. However, a positive definite distribution may be obtained through the procedure of coarse graining the Wigner function with that of a coherent state, which then allows more direct comparisons with classical phase space.[7] Throughout the paper we shall refer to the coarse-grained Wigner function as simply the Wigner function (or wave packet) for brevity. Recently, this technique was used to demonstrate a dramatic correspondence between the classical surface of section and the quantal equivalent for the system of the kicked rotor.[7] This problem, like the present one, displays the transition from regular to irregular motion and the agreement was shown in both regions. Before proceeding, however, an important difference between the two problems is worth appreciating. In the case of the kicked rotor the Wigner function can be expressed in the quantum action-angle representation.[7] It is nontrivial to do this in our case. This leads to a far less dramatic

comparison between classical and quantal phase space and interpretation is restricted to wave-packet dynamics.

In this paper we are particularly interested in addressing an important aspect of the microwave ionization problem. The enhanced ionization seen by experiment has been understood in terms of a diffusive mechanism,[9] arising from the transition of the classical motion from periodic to aperiodic behavior. With increasing frequency Ω, important differences have been reported[9] between the classical and quantum behavior. The threshold for this is best expressed in terms of a scaled frequency,[3] Ω_0, which is defined as the ratio of the external frequency to the classical orbit frequency. This purely classical scaling leads to $\Omega_0=[\Omega(\text{a.u.})]/n_0^3$, where n_0 is the principal quantum number of the initial state. For values of Ω_0 greater than one, the quantum evolution exhibits diffusive behavior only at field strengths higher than those predicted classically. This is a consequence of quantal interference effects and the evolution, for fields lower than a critical value, has been described as localized.[9] The criterion for localization is obtained by mapping the quantal distribution to the solutions of a Fokker-Planck equation.[9] Here, we address the question of whether diffusive behavior is at all present at higher frequencies, in the quantal case, by studying the time development of the Wigner function. This is done by contrasting the evolution with that at lower frequencies as well as the corresponding classical evolution.

It has also been conjectured that quantal localization occurs due to the presence of classical barriers to diffusion.[9] One such scenario invokes invariant nonperiodic trajectories or cantori as these barriers. Cantori possess gaps through which classical motion can diffuse. But, if the size of these gaps is less than h^N (where N is the number of degrees of freedom), it has been shown that cantori act as barriers for quantal evolution.[10] Ideally, the Wigner function can be used to test such scenarios, but locating cantori in the classical dynamics is extremely difficult. Consequently, in this paper, we will concentrate on analyzing the quantal phase-space structures with only qualitative reference to the ideas mentioned.

The paper is formatted as follows. In Sec. II we construct the Wigner function for the unperturbed surface-state electron (SSE) Hamiltonian and describe the numerical calculation of the perturbed problem. Section III discusses the preliminaries which include choice of the coarse-graining parameter, use of a finite basis in the quantal evolution, and interpretation of the Wigner function plots. We discuss the results of our study of the dynamics in Sec. IV. The time evolution of the Wigner function for varying frequency and field strength is considered within the context of a diffusive scenario and of localization at higher frequencies. We conclude in Sec. V with a discussion of the limitations of this procedure and possible improvements as well as future work.

II. CALCULATIONS

The surface-state electron Hamiltonian[3,9] subject to an external perturbation offers a simple, low-dimensional model system with which to test ideas of classical stochasticity. Discussions of the relevance of the SSE Hamiltonian to microwave ionization experiments and comparisons with higher-dimensional versions exist in the literature (see Refs. 3, 8, and 9, for example). In this paper, we treat the SSE as simply a model system in which the classical and quantal dynamics are compared and contrasted. This motivation precludes any detailed discussion of issues relevant to comparison with particular experiments, like field switching and the presence of additional fields.

The unperturbed Hamiltonian is given by

$$H_0(x,p)=\frac{p^2}{2}+\begin{cases}-1/x, & x>0\\ \infty, & x\le 0\end{cases} \tag{1}$$

while the perturbation is of the form

$$V(x,t)=-Fg(t)x\sin(\Omega t)\ , \tag{2}$$

where F and Ω are the peak amplitude and frequency of the microwave field. $g(t)$ represents an envelope function for the field amplitude. For all the calculations reported here, $g(t)=\Theta(t)$, implying a sudden turn on and off. It will be seen that the method developed here is in no way restricted to this particular choice, and the generalization to arbitrary $g(t)$ is trivially accomplished. An additional d.c. field is also sometimes present but that too can be included in a straightforward manner. Atomic units are used in all the equations throughout this paper except when specifying the external field and frequency when the scaled variables $F_0=n_0^4F$ and $\Omega_0=n_0^3\Omega$ are used.[3] As mentioned earlier, these are classical scaling rules but they facilitate demarcating the regular-irregular transition as well as comparison with other works.

The unperturbed bound-state wave functions satisfying the SSE Schrödinger equation are

$$\phi_n(x)=\frac{2}{n^{3/2}}\rho e^{-\rho}L_{n-1}^{(1)}(2\rho)\ , \tag{3}$$

where $\rho=x/n$ and $L_{n-1}^{(1)}$ is the associated Laguerre polynomial[11] and n is the principal quantum number. The wave functions, $\phi_n(x)$, are the same as $R_{nl}(x)/x$ for $l=0$, where R_{nl} is a radial hydrogenic function and x has been substituted for r.

The Wigner function defined for a coordinate space wave function ψ is[4]

$$W(x,p)=\frac{1}{\pi}\int dq\,\exp(-2ipx)\psi^*(x+q)\psi(x-q)\ . \tag{4}$$

Smoothing or coarse graining with another Wigner function yields a positive definite distribution function. A form of coarse graining that has a simple interpretation uses a coherent state wave function[7]

$$\Phi_\alpha(x)=\left[\frac{\omega}{\pi}\right]^{1/4}\exp\left[-\frac{\omega}{2}(x-q)^2+ip\left[x-\frac{q}{2}\right]\right]\ , \tag{5}$$

where $\alpha=\sqrt{\omega}(q+ip/\omega)$ and ω is the coarse-graining parameter. Thus, the coarse-grained Wigner function is defined as

$$\Psi(q,p)=\int\int dp\,dq\; W_{\psi}(q,p)W_{\Phi}(q,p)\;, \tag{6}$$

where W_{ψ} and W_{Φ} represent the Wigner functions of ψ and Φ_{α}, respectively. It can easily be shown that, in this case,

$$\Psi(q,p)=|\langle\psi|\Phi_{\alpha}\rangle|^2\;, \tag{7}$$

where the q and p dependence is contained in the parameter α [cf., Eq. (5)]. Ψ is now a positive definite function that can be interpreted as a probability density. By expanding the Laguerre polynomial in Eq. (3) as a power series in x and integrating each term, we obtain

$$\langle\phi_n|\Phi_{\alpha}\rangle=\frac{1}{2\sqrt{n}}\left[\frac{\omega}{\pi}\right]^{1/4}\exp\left[\frac{-p^2}{2\tilde{\omega}}-\frac{q}{n}-\frac{ip}{\tilde{\omega}}+\frac{1}{2\tilde{\omega}}\right]\times\sum_{m=0}^{n-1}(-1)^m(m+1)\begin{bmatrix}n\\ n-m-1\end{bmatrix}\times\left[\frac{4}{\tilde{\omega}}\right]^{(m+2)/2}\exp(-z^2/4)D_{-(m+2)}(z)\;, \tag{8}$$

where $\tilde{\omega}=n^3\omega$, $z=(1-q\tilde{\omega}-ip)/\sqrt{\tilde{\omega}}$, and D_{-m} is a parabolic cylinder function.[11] In all the equations $\hbar$ has been set to 1 (atomic units). At this juncture, it should be stressed that we do not use $\hbar$ as a parameter to get the classical limit, but rather look at the quantum-mechanical wave packet dynamics associated with $\hbar=1$.

To study the interaction with the oscillatory electric field we need the Schödinger wave function $\psi(t)$ of the full Hamiltonian, $H=H_0+V(t)$. We get ψ by a close-coupling calculation as described in Ref. 12. We will outline the procedure here for completeness and as a reference for further discussion.

The solution to the time-dependent Schrödinger equation may be obtained numerically through an expansion in ϕ_n

$$\psi(t)=\sum_n c_n(t)\phi_n e^{-iE_n t}\;, \tag{9}$$

where E_n are the unperturbed energies. For studying the long-time dynamics, it is simpler to exploit the periodicity of the Hamiltonian to construct and diagonalize the one-cycle time evolution operator U such that $c(T)=U(T,0)c(0)$ where $T=2\pi/\Omega$. The eigenvalues, $\exp(i\omega_a)$, and eigenvectors, ψ_a, of U are given by

$$U\psi_a=e^{i\omega_a}\psi_a \text{ and } \psi_a=\sum_n A_m^a\phi_n\;. \tag{10}$$

The time-averaged transition probabilities are easily expressed in terms of ψ_a. This procedure is, however, limited to sudden switching of the field and hence, to maintain generality, we construct the dynamics in terms of the expansion coefficients $c_n(t)$. The classical transition from regular to irregular motion is manifest both in the distribution of the eigenvalues ω_a (Ref. 13) and in the projection of ψ_a shown in Eq. (10).[12] However, neither is a direct indicator of the extent of similarity between classical and quantal dynamics and, to reiterate, there is evidence of some significant differences.[9]

Having obtained the coefficients $c_n(t)$ by numerical integration, the time evolution in phase space is easily realized. Using the expansion (9) we find

$$\Psi(q,p,t)=|\langle\psi(t)|\Phi_{\alpha}\rangle|^2=\sum_{n,m}c_n^*(t)c_m(t)\Phi_{nm}e^{-i(E_m-E_n)t}\;, \tag{11}$$

where $\Phi_{nm}=\langle\Phi_n|\Phi_{\alpha}\rangle\langle\Phi_{\alpha}|\phi_m\rangle$ and is the coarse-grained equivalent of a Moyal function.[14] The quantal phase-space dynamics may be studied using $\Psi(q,p,t)$. The eigenvectors ψ_a of the time evolution operator can be similarly treated using the expansion (10) to get

$$|\langle\psi_a|\Phi_{\alpha}\rangle|^2=\sum_{n,m}A_n^{a\,*}A_m^a\Phi_{nm}\;. \tag{12}$$

It is clear that coherence effects due to quantum interference occur through the summations in (11) and (12). Structures in the quantal phase space, during the course of evolution, are a consequence of these effects.

III. PRELIMINARY ASPECTS

Before discussing the results, there are a few aspects of this treatment that need to be clarified. Numerical tractability forces the choice of an incomplete basis set for the expansion (9) and finite basis effects can appear.[12] The main consequence is reflection of probability if the evolution encounters the end of the basis. By choosing a large basis and by restricting the time of evolution, finite basis effects can be minimized. Also by varying the size of the basis, we have verified that the conclusions of this paper are not affected by the use of a finite basis. A related issue is our exclusion of the continuum in the expansion (9). This is justified partly by our interest in the transition from regular to irregular dynamics within the bound states. Further, calculations using Sturmians and box-normalized continua point to the negligible role of the continuum for the field parameter values we consider.[15]

As mentioned earlier, the value of $\hbar$ is 1 for all the results presented in this paper. This is in contrast to most other studies that use the Wigner function to examine quantum systems whose classical analogues are nonintegrable. In these, $\hbar$ is used as a parameter in order to semiclassically resolve structures in classical phase space. However, having $\hbar=1$ is consistent with our purpose of looking for strictly *quantal* analogues of classical stochasticity.

It is useful at this juncture to discuss the motivation for the choice of parameters. We begin with our choice of the coarse-graining parameter ω. The driven-SSE system is examined by an expansion of its Wigner function in terms of Moyal functions of the unperturbed system. Thus, ω must be chosen for the *hydrogenic* Moyal or, equivalently, *hydrogenic* Wigner function. For the coherent state, ω represents the frequency of a corresponding harmonic oscillator. The natural frequency for a surface-state electron in a state labeled by a principal

quantum number n is $1/n^3$. Setting ω to be the natural frequency of the unperturbed system was proposed and discussed by Husimi,[16] in the context of thermodynamic Wigner functions. Though the applicability of Husimi's analysis to this case is unclear, this choice of ω appears intuitively correct for this problem. Criteria for the choice of ω can be obtained from the uncertainty relations for q and p, as ω determines the extent of quantal fluctuations for the coherent state. For the coherent state, (5),

$$\Delta q = \sqrt{\hbar/2\omega} \text{ and } \Delta p = \sqrt{\hbar\omega/2}. \tag{13}$$

For the coarse-grained Wigner function the widths are given by[17]

$$(\Delta q)_\Psi^2 = (\Delta q)_n^2 + \frac{1}{2\omega} ,$$
$$(\Delta p)_\Psi^2 = (\Delta p)_n^2 + \frac{\omega}{2} , \tag{14}$$

where Ψ designates the coarse-grained Wigner function and n the nth hydrogenic state. Further, $(\Delta q)_n^2 \sim n^4$ and $(\Delta p)_n^2 \sim n^{-2}$. From (14) we see that the two widths are approximately equal if the following condition is satisfied:

$$\frac{1}{2n^4} \ll \omega \ll \frac{2}{n^2} . \tag{15}$$

The choice of $\omega = 1/n^3$ ensures (15) for large n. Obviously, this choice is not unique, and this fact will be used later in the discussion.

In order to clearly demonstrate the effect of varying the coarse-graining parameter, Fig. 1 shows the Wigner function for the unperturbed SSE for three representative values of ω; $\omega = 0.01\omega_n$, ω_n, and $100\omega_n$, respectively, where $\omega_n = 1/n^3$. The range of variation of x is 0 to 25 000 a.u. and the range in p is -0.05 to $+0.05$ a.u. The Wigner function plotted is for the state with principal quantum number $n = 63$. In units of ω_n, $\omega = 1$ [Fig. 1(c)] is the case that has been used for all calculations reported in this paper. Also shown for comparison, in Fig. 1(d), is a classical trajectory for initial action corresponding to the quantum state $n = 63$. It is clear that the $\omega = 1$ case best corresponds to wave packet described above. The peak occurs at $p = 0$ where the electron spends most of its time and for large momenta, we see that the Wigner function trails off. For the cases of ω not equal to the natural frequency, we see that the wave packet is "squeezed"; the width in p or q is exaggerated depending on ω being greater than or less than $1/n^3$. This clearly demonstrates that $\omega \approx \omega_n$ is the proper coarse graining for the unperturbed SSE Wigner function. This also shows that at $t = 0$ we get correspondence between quantal and classical phase space. Any differences that develop at later times are, thus, a consequence of the dynamics.

In the expansion (11), we cannot have $\omega = 1/n^3$ for every n in Φ_{nm}; a specific ω must be chosen. We use

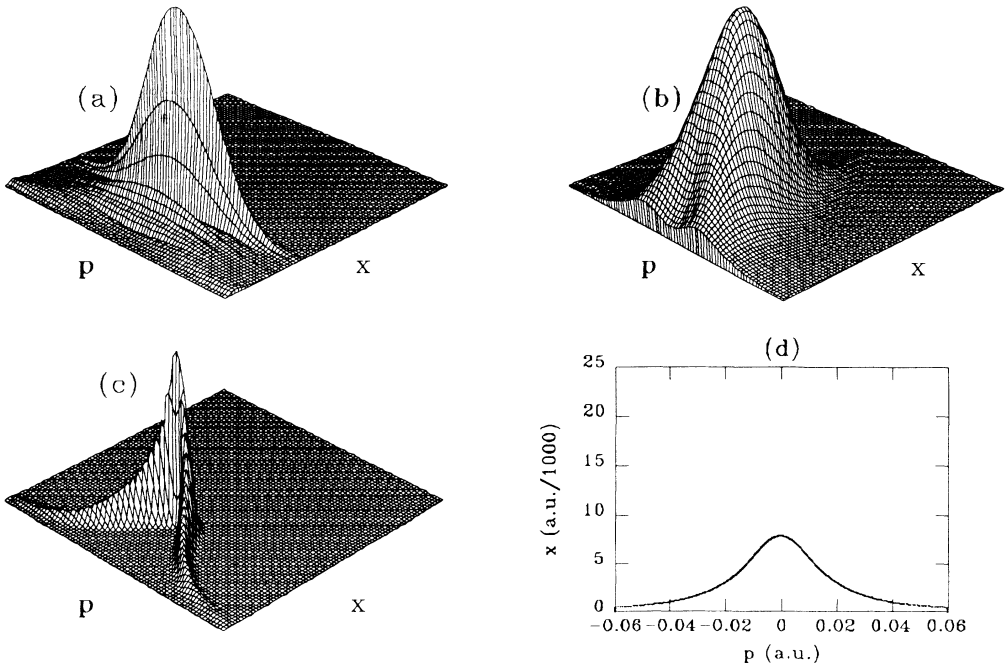

FIG. 1. Quantal phase-space density as a function of the coarse graining. The coarse-graining parameter ω is in units of ω_n where $\omega_n = 1/n^3$. n (=63) is the principal quantum number. The value of ω is (a) $0.01\omega_n$, (b) $100.0\omega_n$, and (c) ω_n. (d) is a classical trajectory for action equal to 63. The axes for the 3D figures are as follows in a.u.: p: -0.05 to $+0.05$ and x: 0 to 25 000.

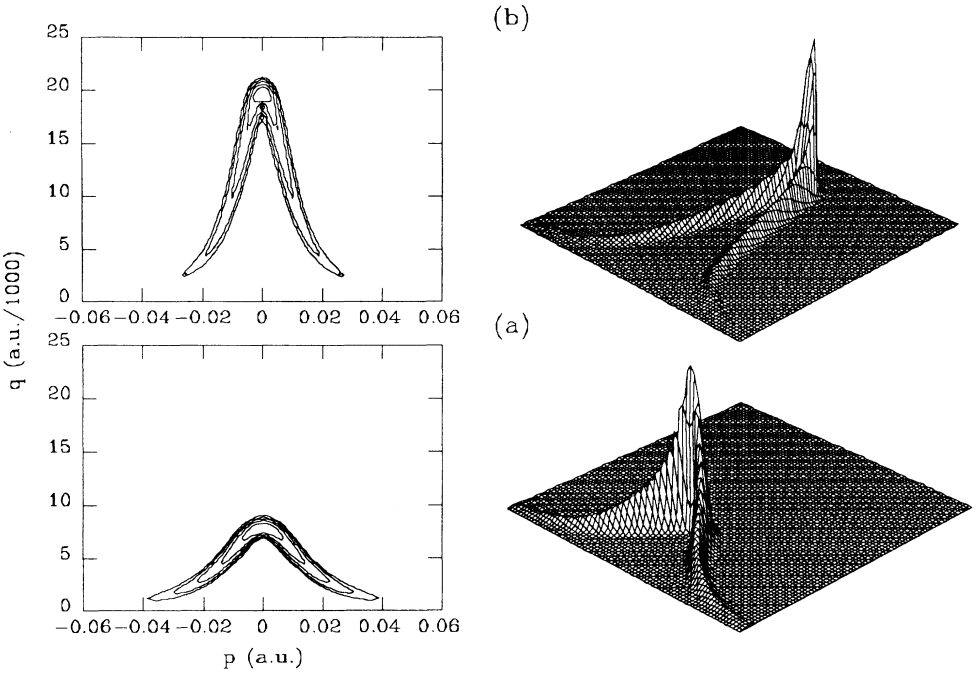

FIG. 2. Unperturbed Wigner function corresponding to quantal states: (a) $n=63$ and (b) $n=100$. The same coarse graining was used in both cases, $\omega=1/63^3$.

$\omega=1/n_0^3$ where n_0 is the quantum number of our initial state. However, (15) gives some latitude in the value of ω, and for our basis we still satisfy (15) by choosing $\omega=1/n_0^3$. To illustrate this and show how the unperturbed Wigner function appears, Fig. 2 shows the unperturbed Wigner functions for $n=63$ and 100 with $\omega=1/63^3$ for both cases. Both the three-dimensional plot and the contour plot of the Wigner function are shown, with the x and p scales shown for the contour plot. In Fig. 2(a), we see the Wigner function peaks at about 8000 a.u. which corresponds well with the classical trajectory in Fig. 1(d). In general, the peak of the Wigner function of an unperturbed n is located at $x=2n^2$ and $p=0$, corresponding to the turning point of the classical trajectory. It can be easily verified that the $n=100$ Wigner function in Fig. 2(b) with peaks at 20 000 a.u. and the $n=63$ peak at 8000 a.u. satisfy this condition.

A few remarks need to be made concerning the range of variation of the Wigner functions shown. The range of x and p used does not completely enclose the entire density distribution. This is seen by the bumps at the edge for large momentum and small position in Fig. 1(c). The range in x and p has been chosen to optimally resolve the important features in phase space. The probability outside this range is smaller than the resolution of our contour plots and no discernible behavior occurs.

All the contour plots show the same set of levels. These are 2×10^{-2}, 9×10^{-3}, 4×10^{-3}, 2×10^{-3}, 8.7×10^{-4}, and 4×10^{-4}. The values of the levels were chosen using a logarithmic scale in order to get the full range of heights. The plot height of all the three-dimensional (3D) plots are not the same but are scaled for maximum resolution. Therefore, the contour levels should be used to determine relative heights. The range of phase space calculated is 0–25 000 a.u. for x and -0.05 to $+0.05$ a.u. for p. These ranges apply both to the contour and 3D plots.

IV. DISCUSSION

In assessing the time evolution of phase-space probability we considered a range of the external field parameters, namely, the frequency and field strength. However, in the course of this discussion we restrict ourselves to a few representative cases to illustrate the features seen. To explore the question of stability we begin by considering the time evolution of the phase-space density corresponding to the initial conditions in the classically regular and irregular regions.[3] Figures 3 and 4 show such an evolution when starting with a Wigner function of the $n=63$ state with field strengths $F_0=0.04$ and with frequencies $\Omega_0=0.3$ and 0.7, respectively. Changing the frequency at this value of the field strength is sufficient to put the initial state above the threshold for classical stochasticity. Figure 3 shows the evolution for an initial condition in the classically regular regime ($\Omega_0=0.3$) while Fig. 4 shows the evolution from an initial condition in the irregular regime ($\Omega_0=0.7$). In units of the external time period $T=2\pi/\Omega_0$, the progression of the wave packet at times $t=0$, T, $5T$, and $10T$ is shown. In the regular regime the evolution produces oscillations in the density distribution with little movement in the position of the central peak. The Wigner function stays in approximately the same region of phase space, but it redistributes itself within that region. In contrast, in the irregular regime, the density evolves to higher values of x (Fig. 4). It

delocalizes to the top of the basis after a very short time, on the order of five cycles. We considered the transition from the regular to irregular regime by varying the frequency so as to maintain the same initial state, $n=63$. For the case $\Omega_0=0.7$, the state $n=55$ is in the classically regular region and we have confirmed that its evolution is like that for the regular state $n=63$ at $\Omega_0=0.3$. It is clear that for these parameter values, the phase-space dynamics shows a dramatic difference when starting in classically regular and irregular domains.

The parameter values considered do not satisfy the condition for the onset of quantal suppression effects.[9] Let us now increase the driving frequency to determine whether the pattern of evolution for quantum states in the irregular regime persists on approaching the localization threshold. In Figs. 4–6, we show the evolution for frequencies $\Omega_0=0.7$, 1.5, and 2.5, respectively. In all three cases the field strength $F_0=0.04$ and the initial condition $n=63$ is in the classically predicted irregular regime. In each case, the figures plot the density at times

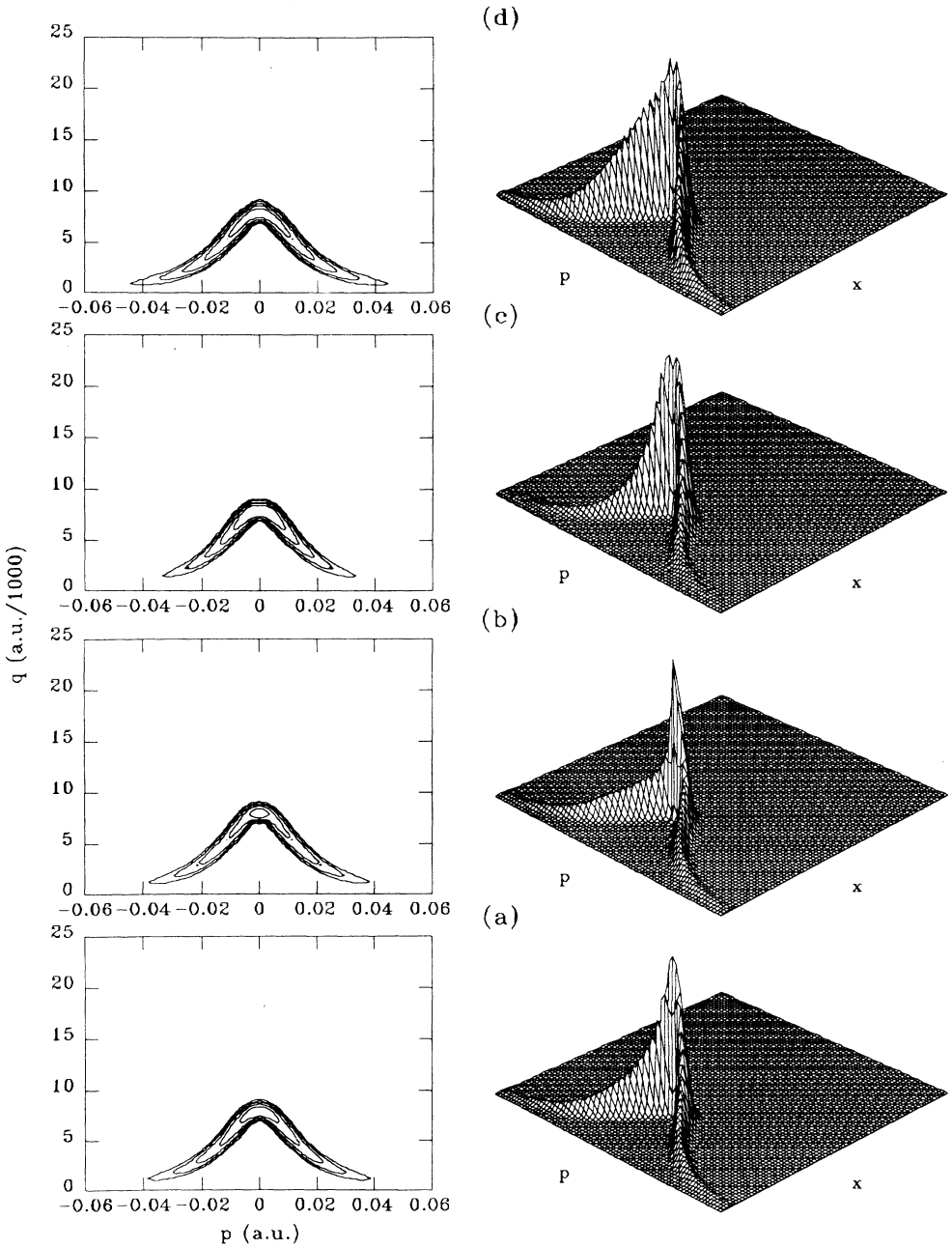

FIG. 3. Time evolution for parameters $F_0=0.04$, $n_0=63$, and $\Omega_0=0.3$. The times plotted are (a) 0, (b) T, (c) $5T$, and (d) $10T$, respectively, where $T=2\pi/\Omega_0$. The initial state is the unperturbed $n=n_0$ state.

$t=0$, T, $5T$, and $10T$ where T is the period of the external field. As we are varying the frequency, the density is not shown at the same physical times. This does not alter any of our conclusions and we demonstrate this a little later by considering the evolution over long times.

Let us now examine the evolution of the phase-space density in detail. Even at the end of a single cycle of the external field the effects of increasing Ω_0 are clearly visible. While the initial state for all cases is peaked at about 8000 a.u. $\cong 2n^2$, part of the $\Omega_0=0.7$ case has evolved in q space to about 10 000 a.u. In contrast, both the $\Omega_0=1.5$ and 2.5 have not evolved at all. In fact, in the case of $\Omega_0=2.5$ there is no perceptible difference between the distributions at $t=0$ and $t=T$. For $\Omega_0=1.5$ the Wigner function has redistributed its probability within the $t=0$ phase-space regime, much like the behavior in the regular regime. It appears that increasing Ω_0 at least slows the flow of the wave packet to increasing q even for very short times.

At the end of five cycles there is a dramatic change in

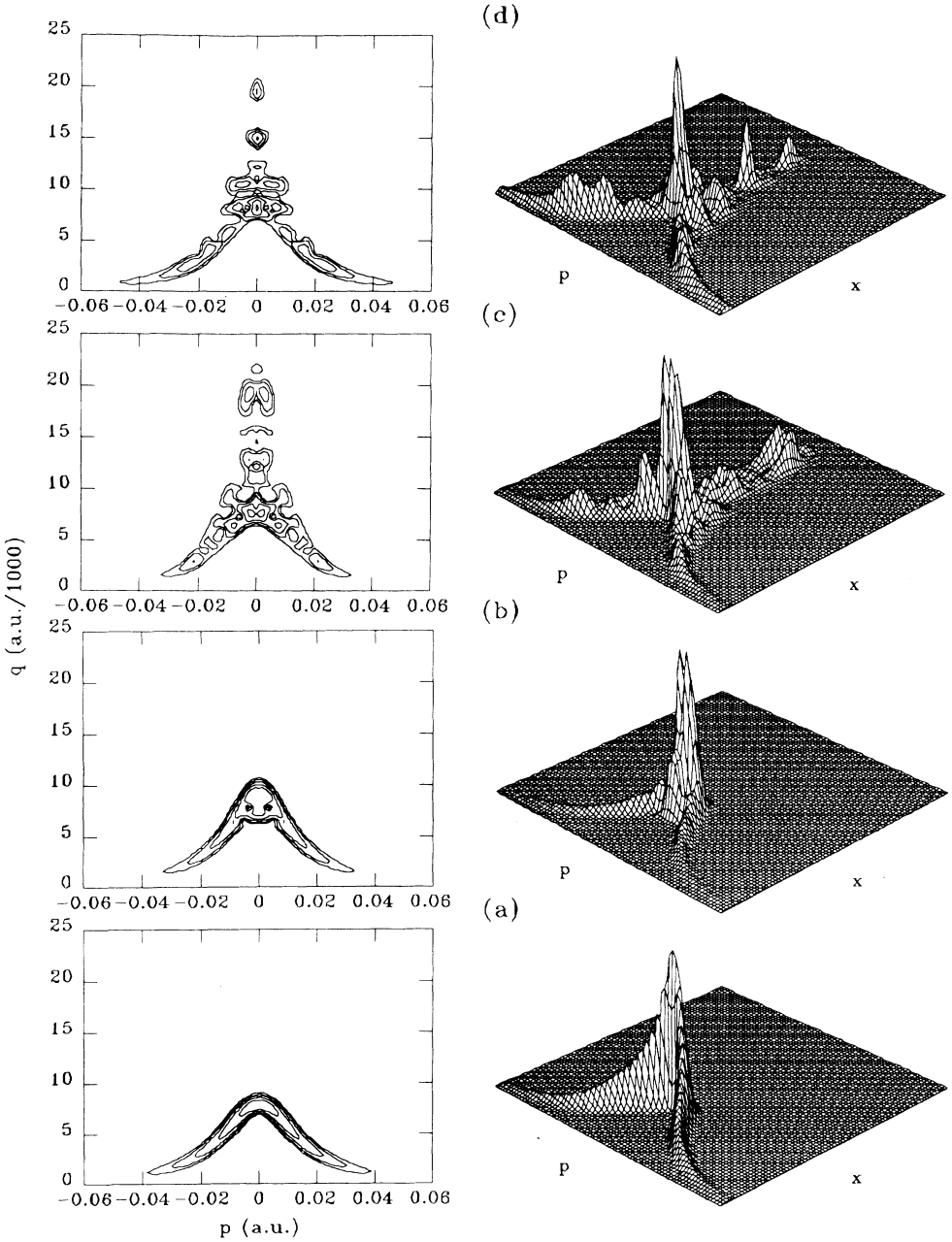

FIG. 4. Time evolution for parameters $F_0=0.04$, $n_0=63$, and $\Omega_0=0.7$. The times plotted are (a) 0, (b) T, (c) $5T$, and (d) $10T$, respectively, where $T=2\pi/\Omega_0$. The initial state is the unperturbed $n=n_0$ state.

the $\Omega_0=0.7$ Wigner function. The phase-space density extends beyond 20 000 a.u., which corresponds to the neighborhood of the $n=100$ state. The initial wave packet separates into smaller wave packets and the propagation of each appears coherent. It should be noted that the size of the small separated parts is significant on the scale of a phase volume. The $\Omega_0=1.5$ case has evolved to about 10 000 a.u. (2×71^2), far less than the previous case. However, the density flow up to 10 000 a.u. is very small; the bulk of the wave packet remains distributed much the same as at $t=0$, although there has been a rearrangement within that region. Here again the similarity with the regular regime is striking. Higher still, at $\Omega_0=2.5$ the center of the wave packet has not appreciably moved. Thus, for $\Omega_0=1.5$ and 2.5 practically no *outward* evolution in coordinate space has occurred after five cycles; the densities only redistribute themselves within the original region of phase space. But for the $\Omega_0=0.7$ case there is significant evolution outward through the splitting of the original wave packet into smaller pieces.

By ten cycles the $\Omega_0=0.7$ Wigner function has encountered the edge of our basis, and therefore we see reflection

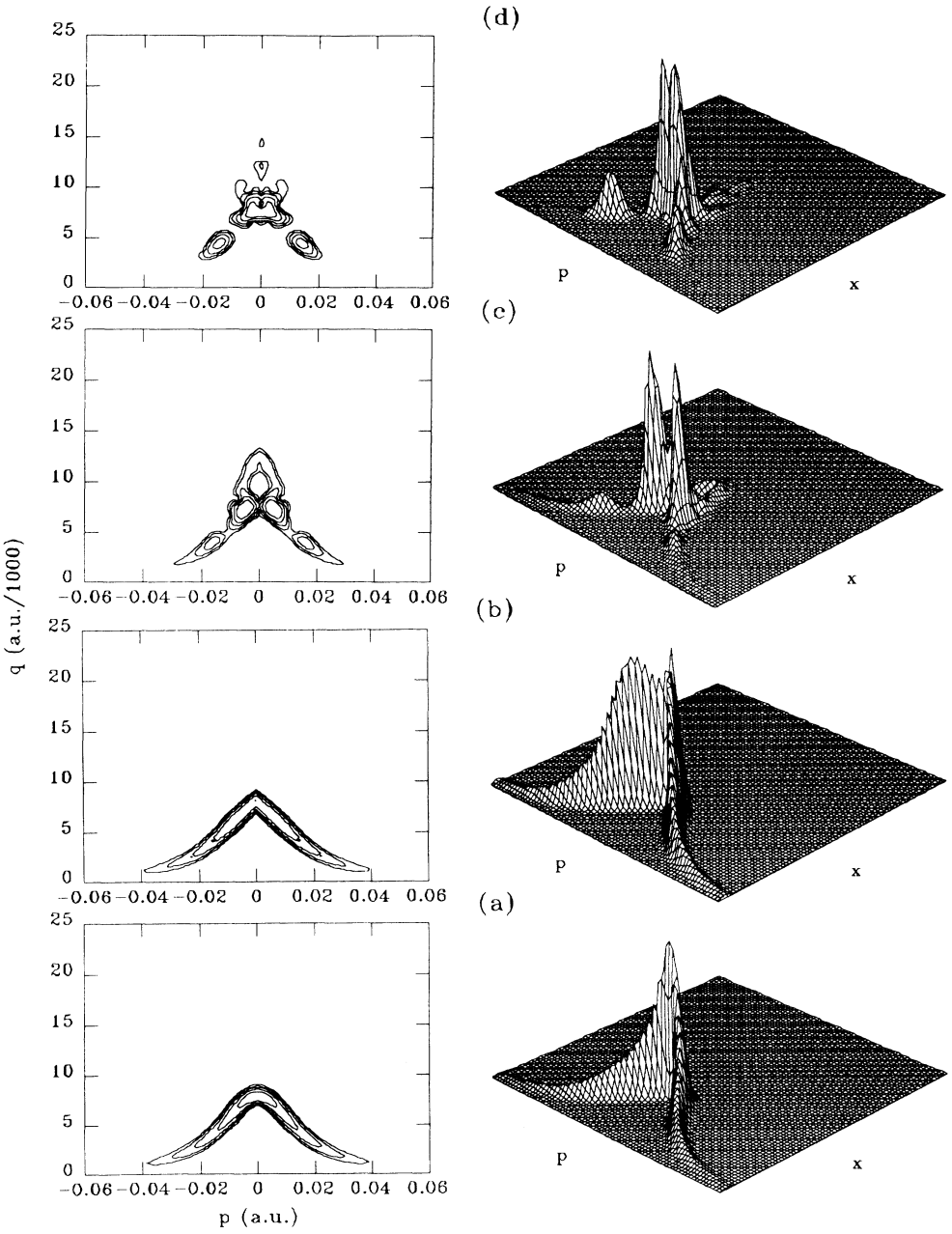

FIG. 5. Time evolution for parameters $F_0=0.04$, $n_0=63$, and $\Omega_0=1.5$. The times plotted are (a) 0, (b) T, (c) $5T$, and (d) $10T$, respectively, where $T=2\pi/\Omega_0$. The initial state is the unperturbed $n=n_0$ state.

effects. For $\Omega_0=1.5$, there is only insignificant flow beyond 10 000 a.u. (2×71^2). The only contour observed is the lowest at 4×10^{-4}. The localization is more pronounced at $\Omega_0=2.5$ where there is no flow at all beyond 10 000 a.u. which corresponds to $n=71$. Therefore, it is already clear that the low-frequency case evolves in q space quite readily in contrast to the higher frequencies. The question now is whether the higher-frequency densities evolve further in q over longer times, or whether they remain localized.

In the cases considered, we confirm the qualitative agreement between the classical and quantal (Wigner function) distributions for short times (up to $10T$), shown earlier.[9] It is, however, on longer time scales that the differences between quantum and classical evolution become apparent. In Figs. 7 and 8 the densities for $\Omega_0=1.5$ and 2.5 are plotted at times $t=20T$, $30T$, $80T$, and $100T$. With these interaction times we have realized the time scales over which Casati *et al.*[9] report differences in quantum and classical behavior.

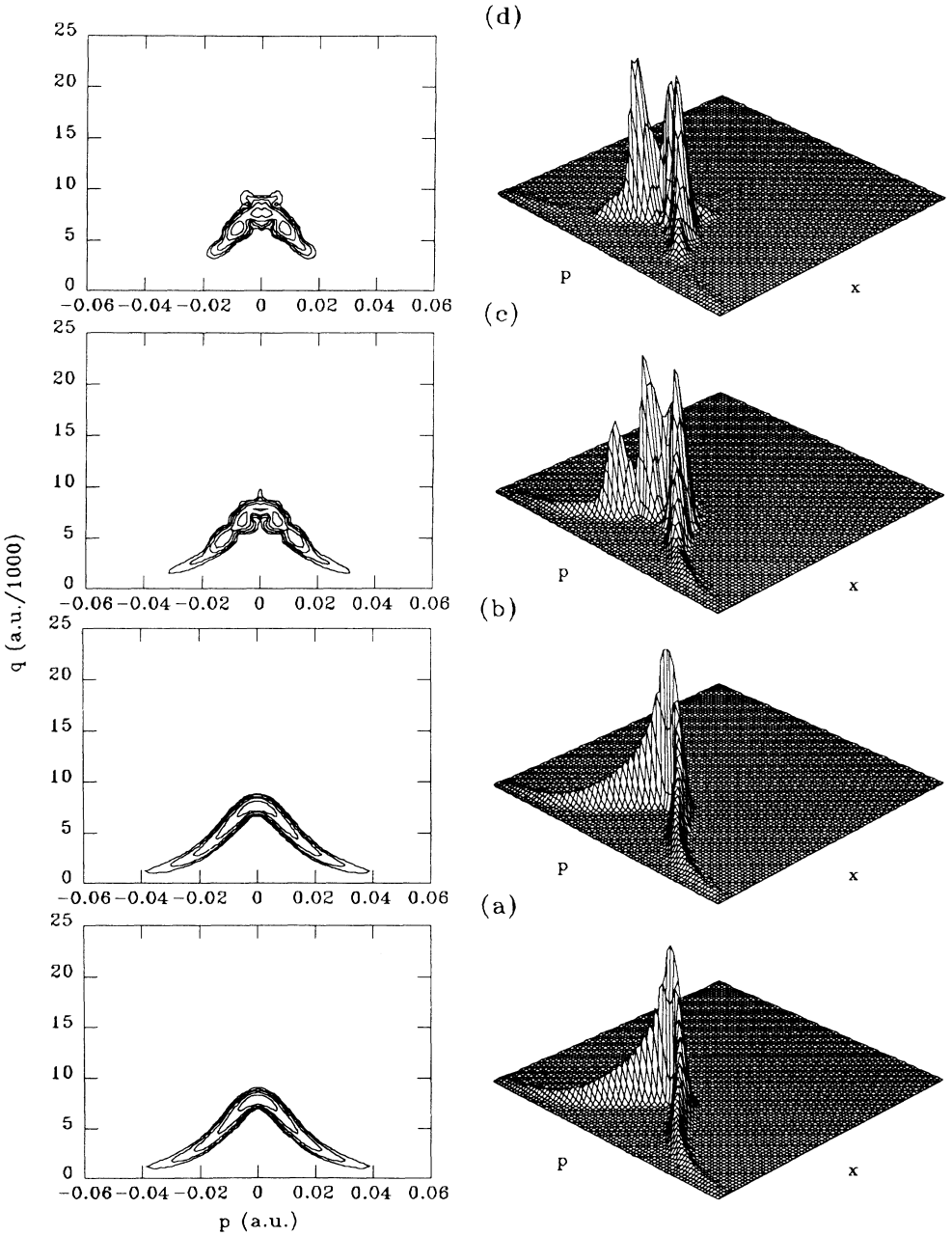

FIG. 6. Time evolution for parameters $F_0=0.04$, $n_0=63$, and $\Omega_0=2.5$. The times plotted are (a) 0, (b) T, (c) $5T$, and (d) $10T$, respectively, where $T=2\pi/\Omega_0$. The initial state is the unperturbed $n=n_0$ state.

Both Figs. 7 and 8 show some evolution beyond 10 000 a.u. for $\Omega_0=1.5$ and 2.5, respectively. By 20 cycles the $\Omega_0=1.5$ plot shows a significant fraction of the density has evolved to just above 10 000 a.u. A discernible piece has reached 18 000 a.u. $\approx 2\times 95^2$ at 30 cycles. By this time, there is a more appreciable fraction from 10 000 a.u. to just above 15 000 a.u. $\approx 2\times 87^2$. The picture does not change much for the longer times of $80T$ and $100T$ except for growth of the peak at 15 000 a.u. All of the structure that has flowed from the original wave packet is of a size larger than h. Going to the $\Omega_0=2.5$ case, the density distribution at $t=20T$ is not qualitatively different from that at shorter times. There is, however, some probability at about 10 000 a.u. After 30 cycles a small fraction of the original wave packet evolves beyond 10 000 a.u., but it is of the order 4×10^{-4} (the lowest level). For both the 80- and 100- cycle plots the furthest extent is 15 000 a.u., but it is very small. There is some evo-

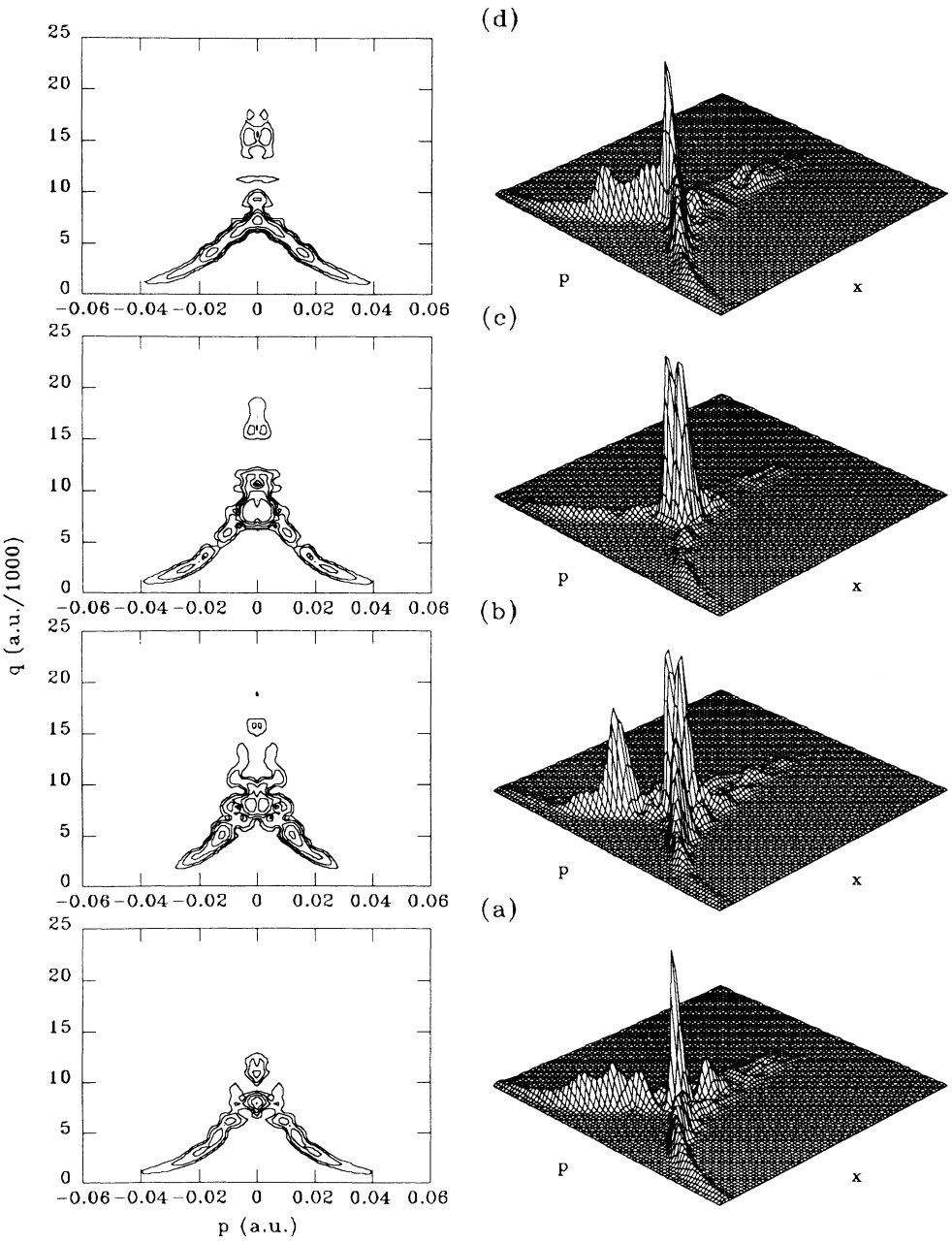

FIG. 7. Parameters same as in Fig. 5. Times considered are $t=20T$, $30T$, $80T$, and $100T$.

lution as seen by the amount of probability ($\frac{1}{10}$ the main peak) at 12 000 a.u. at $t=100T$.

While there is some flow to higher values of q in Figs. 7 and 8, it is not of the same magnitude as that seen in the $\Omega_0=0.7$ case in just five cycles. By this time in the 0.7 case the distribution had reached the end of our basis. The higher-frequency cases do not achieve this even at the end of $100T$. Thus, a factor of 2 or 3 change in frequency leads to more than a factor of 20 in evolution times. It would seem that the time scales for the high-frequency evolution are disproportionately longer than the low-frequency cases.

Let us now consider the classical dynamics over the time scales shown in Figs. 7 and 8. We have plotted in Figs. 9 and 10 the classical Poincaré sections at times $20T$, $30T$, $80T$, and $100T$, for frequencies $\Omega_0=1.5$ and 2.5, respectively. The plots are in x and p although the dynamics was evaluated in an action-angle representation,[18] as this is more consistent with our strictly bound-state quantum evolution. The plots were created using

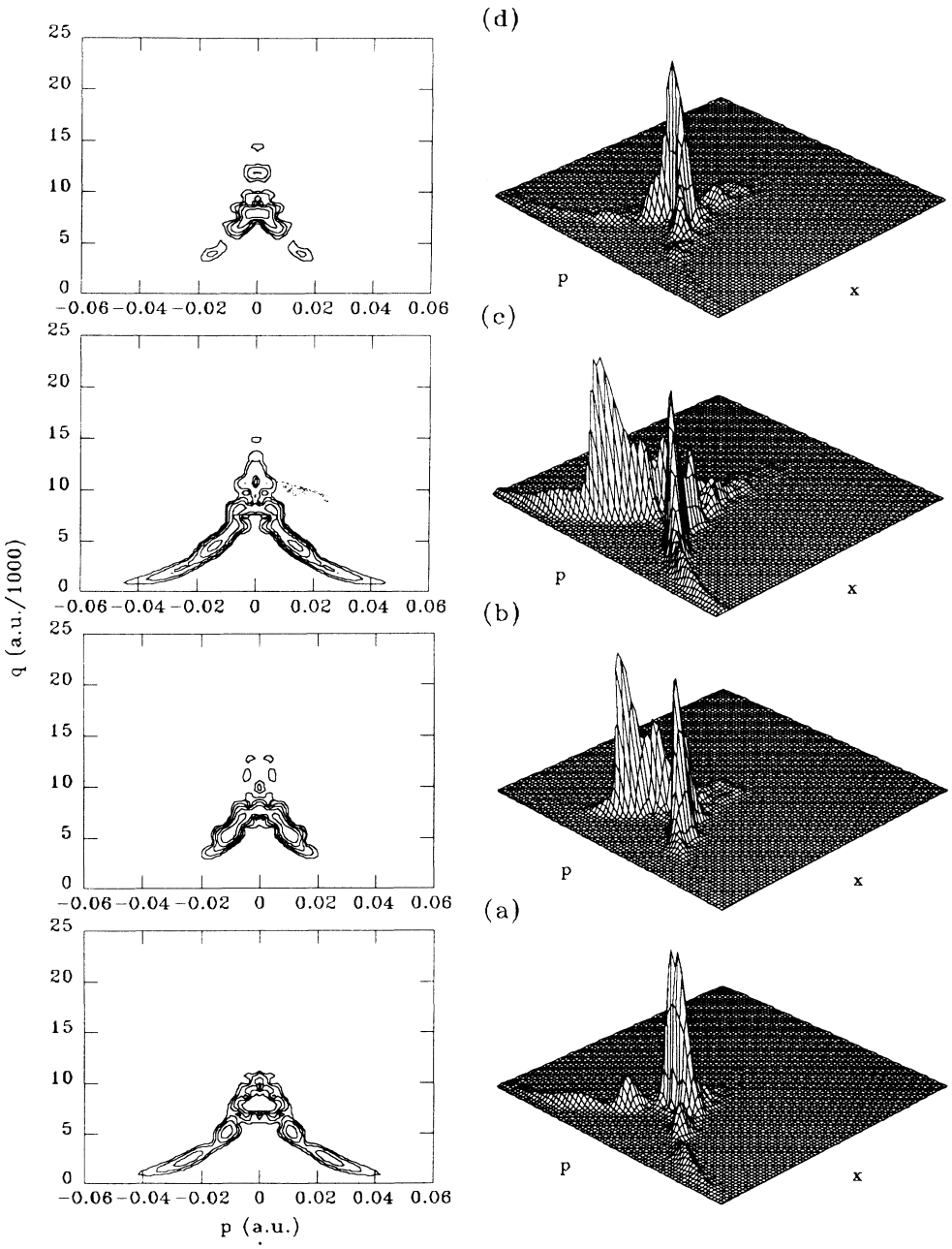

FIG. 8. Long-time evolution for $\Omega_0=2.5$. Other parameters are the same as Fig. 6. Times are $t=20T$, $30T$, $80T$, and $100T$.

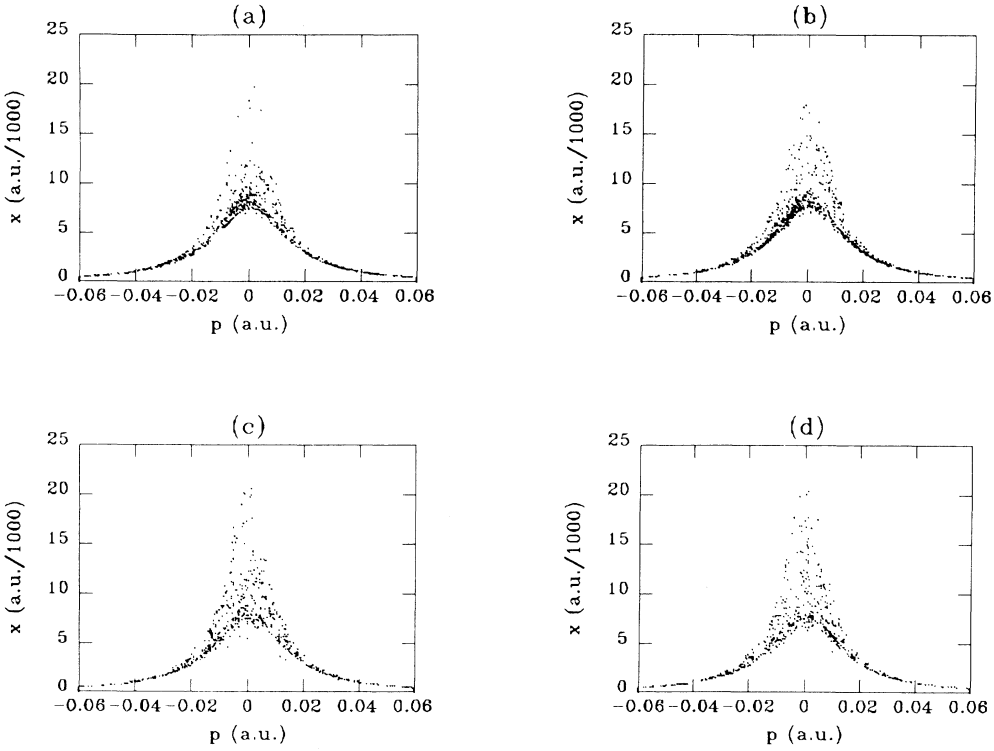

FIG. 9. Classical phase-space portraits corresponding to the quantum plots of Fig. 8. The initial distribution was 1000 angles at an action of 63. The parameters and times are the same as in Fig. 8.

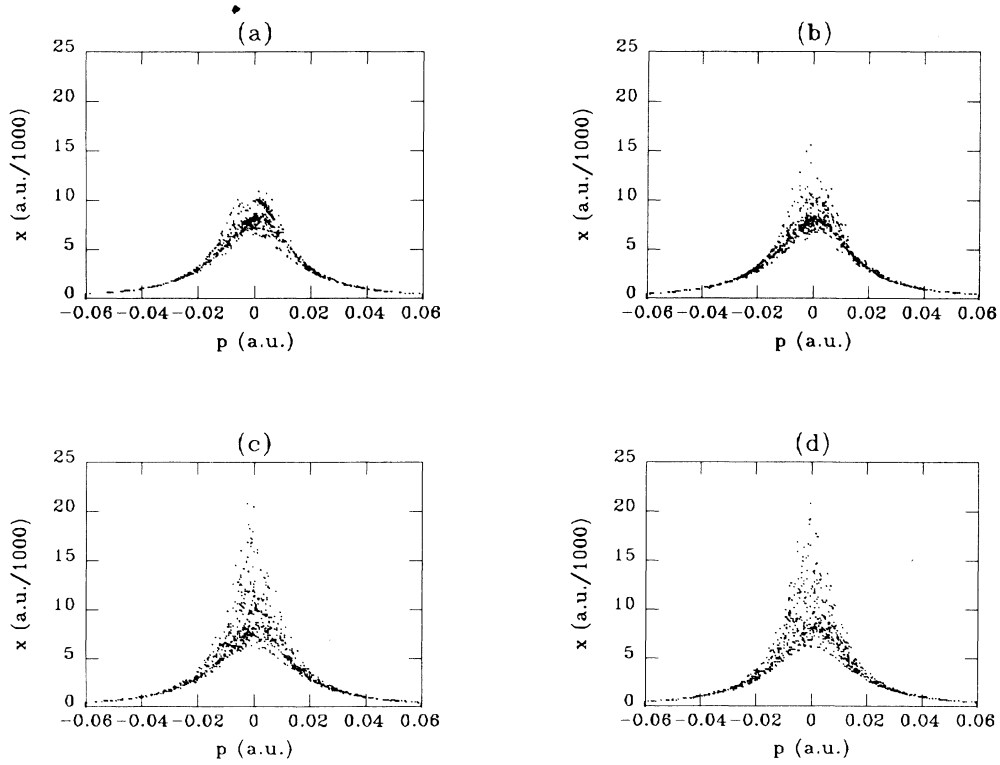

FIG. 10. Classical phase-space distributions corresponding to the quantum plots of Fig. 9. The initial distribution was 1000 angles at an action of 63. The parameters and times are the same as in Fig. 9.

1000 initial values of the angle evenly distributed at an action $I_0=63$. This classical ensemble corresponds to the quantal initial condition. A cutoff at a scaled action $I/I_0=1.7$ has been imposed; this corresponds to an unscaled action which approximates the top of our quantum basis.

Classically, after an equal number of cycles the $\Omega_0=2.5$ case is more stable than the $\Omega_0=1.5$ case. A measure of excitation is the number of trajectories that are excited above our cutoff by the end of the interaction time. After $100T$ the $\Omega_0=2.5$ case has 48 of 1000 trajectories above the cutoff of 1.7, while the $\Omega_0=1.5$ case loses 447 of 1000 trajectories. Furthermore, the classical dynamics reaches the equivalent of the end of the basis ($I=1.7$) after 40 cycles for $\Omega_0=2.5$ and after 20 cycles for $\Omega_0=1.5$; even at times shorter than $100T$ the classical evolution extends far further than the quantal evolution.

The differences between the classical and quantal dynamics can now be illustrated. Neither the $\Omega_0=1.5$ or 2.5 quantal densities reach the end of the basis after 100

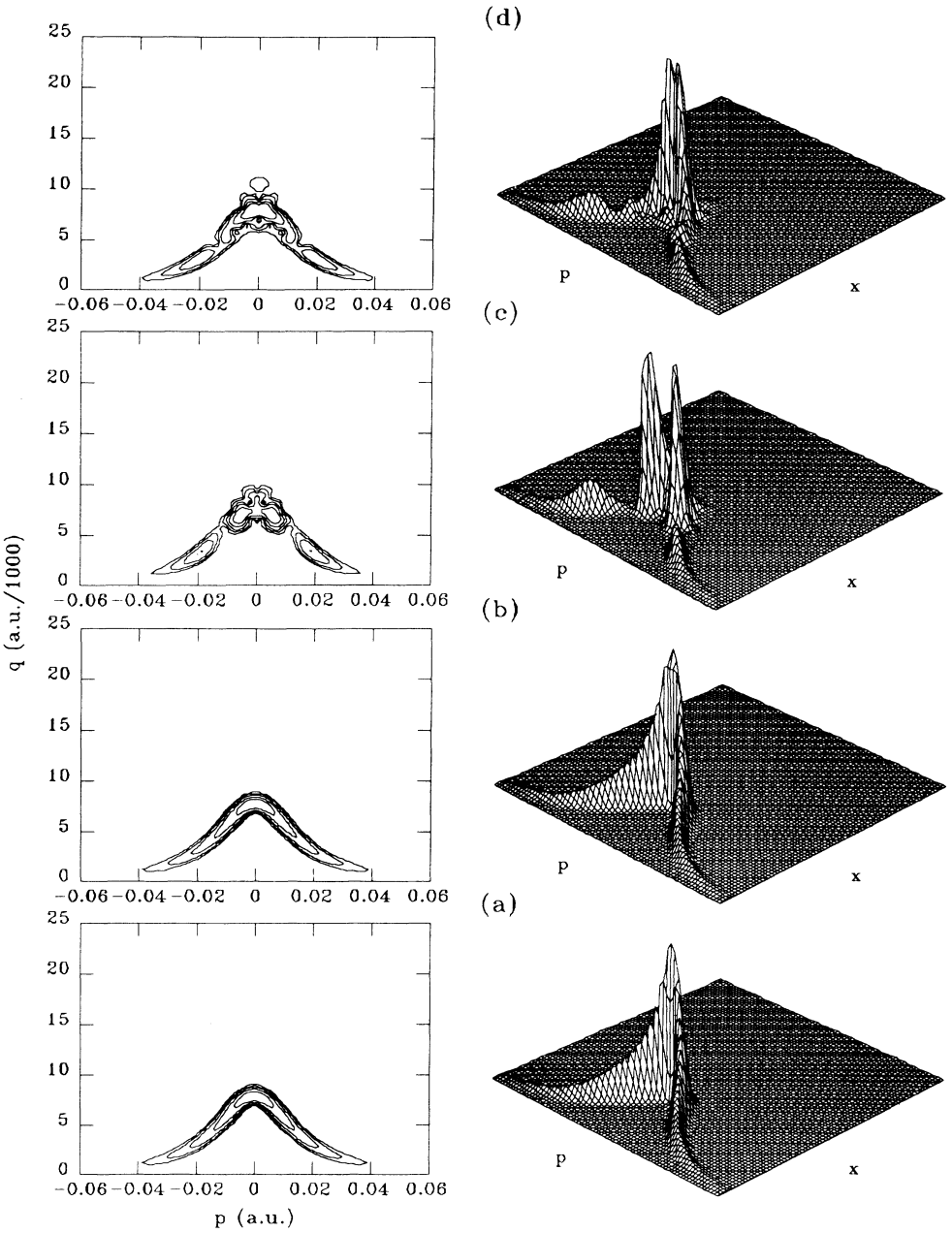

FIG. 11. Time evolution for parameters $F_0=0.05$, $n_0=63$, and $\Omega_0=3.4429$. The times plotted are (a) 0, (b) T, (c) $5T$, and (d) $10T$, respectively, where $T=2\pi/\Omega_0$. The initial state is the unperturbed $n=n_0$ state.

cycles. This disparity is most evident in the $\Omega_0=1.5$ case where 45% of the classical trajectories go beyond $I=1.7$. For there to be such a significant fraction of the quantal phase-space density above the top of our basis the main peak must move. No such movement of the main peak has been observed. Even to achieve the smaller 5% evolution for $\Omega_0=2.5$ case would require a substantial peak near the top of the basis. This demonstrates a significant difference between the classical and quantal high-frequency evolution. In relation to the classical evolution, the quantal evolution out of the initial phase-space region is inconsequential.

We have, so far, considered only one field strength, $F_0=0.04$. We now briefly comment on some of the effects of the field strength on the Wigner function. In Figs. 11 and 12 we show the time evolution of the cases $F_0=0.05$ and 0.15 with $\Omega_0=3.4429$ with the same initial state, $n=63$. Increasing the field strength from 0.05 to 0.15 causes resonant structures present in the 0.05 case to disappear.[19] It is these structures that present classical

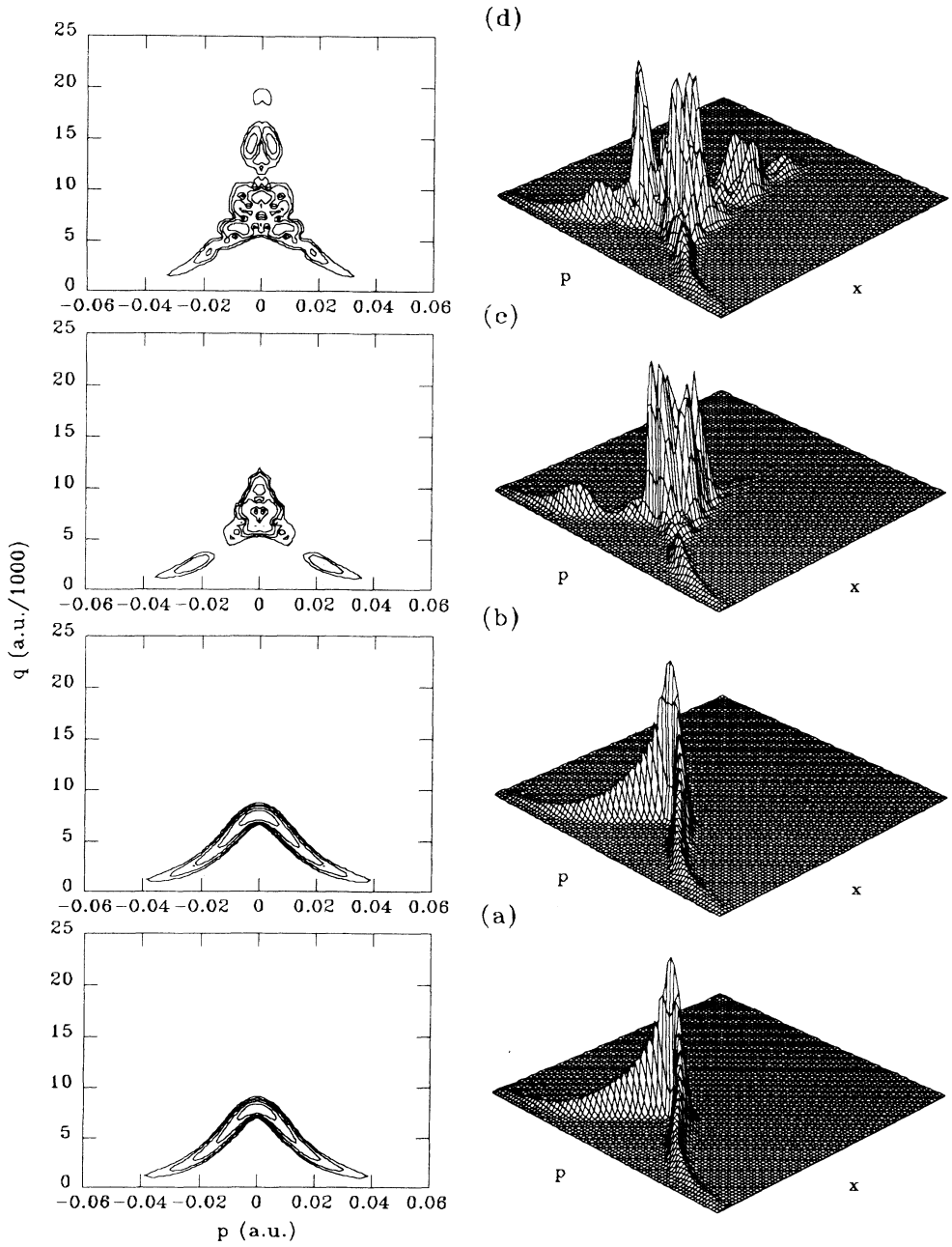

FIG. 12. Same as Fig. 11 except at a higher field $F_0=0.15$.

barriers to diffusion in the 0.05 case. The times considered in Figs. 11 and 12 are $t=0$, T, $5T$, and $10T$. For the $F_0=0.05$ case the wave packet does not move but rearranges itself within the same region of phase space. This conforms with the behavior observed above for the high-frequency cases. However, the $F_0=0.15$ case is quite different. We see a very large peak at 10 000 a.u. in the $5T$ plot [Fig. 12(c)]; this peak's size is of the same order as the initial peak remnant at 8000 a.u. After ten cycles there is still a large peak at 10 000 a.u. together with a smaller but significant peak at 15 000 a.u. We see here behavior reminiscent of the $\Omega_0=0.7$ case. Even though this is a high-frequency case, we are seeing evolution of the wave packet to higher q values. This case was included to illustrate that all aspects of this problem can be addressed in this formulation.

V. CONCLUSIONS

We have examined the evolution of the phase-space density for the driven SSE Hamiltonian using a coarse-grained Wigner function. Our primary motivation was to assess the dynamics in different frequency regimes, both for short and long times, for initial conditions chosen within regular and irregular regions in classical phase space. We confirm that for higher frequencies, and parameters satisfying the criterion for suppression,[9] the quantal evolution is predominantly localized within the initial region of phase space. An increase in the evolution time by a factor of 20 relative to a increase in frequency by a factor of 2 or 3 does not yield significant movement of the wave packet. This is in sharp contrast with the classical dynamics which shows diffusive flow. In fact, the quantal, high-frequency behavior is reminiscent of the evolution of a wave packet in a classically regular part of phase space, which is constrained by the presence of invariant tori.

There are two alternative scenarios that have been proposed to explain the quantal suppression effects seen at higher frequencies. One is the localization theory[9] which is a consequence of quantal interference, while the other relates to the presence of classical barriers to evolution. This second picture would have the quantal evolution occurring by tunneling through classical barriers present in phase space. Localization effects result in the probability distribution, over energy eigenstates, being an exponentially decaying function.[9] In our formulation, this is reflected in the expansion coefficients $c_n(t)$ [Eq. (11)] and, hence, in our phase-space distributions. In principle, our long-time evolution of the phase-space densities should allow an assessment of the relative merits of these theories. The localization picture requires a measure of the time-dependent flow whereas the cantori effects would be seen in the size of the smaller wave packets. We were, however, unable to construct an unambiguous quantitative measure of either quantity and so restrict ourselves to a qualitative assessment.

In the localization scenario, a measure of quantal inhibition is a characteristic length l. This parameter, in turn, provides an estimate of the upper time bound τ_b (in units of field cycles) for diffusion.[9] τ_b is interpreted as the time beyond which quantum effects localize the evolution. For our high-frequency cases, the values of the so-called *break time* τ_b are 4.9 and 1.5 for Ω_0 of 1.5 and 2.5, respectively. These values predict diffusion on time scales comparable to those considered in Figs. 5 and 6. However, the flow observed is on time scales longer than those predicted (Figs. 7 and 8).

In the cantori (classical barriers) scheme, the nature of the evolution is related to the size of "turnstiles"[20] or gaps in the cantori. When the cantori gaps get too small (with respect to h) for the quantum wave packet to diffuse through, the evolution is restricted to tunneling through the cantori barriers. It is interesting that estimates of the cantori gaps[20] are consistent with our long-time observations. They are smaller than h for both the 1.5 and 2.5 cases though larger for $\Omega_0=0.7$. Thus, for the lower frequency when the cantori gaps are large on the quantum scale, we see what appears diffusive, but at the higher frequencies when the gaps get smaller, we see a much slower flow. This is manifest in the time scales over which the flow occurs.

We would like to conclude with a few comments on some limitations of this approach. The Wigner function calculated here is a function of Cartesian variables. As mentioned, classical phase space is better mapped in an action-angle representation. This has been illustrated convincingly for the kicked-rotor problem.[7] This would also provide a better topological understanding of the dynamics in terms of local invariances. Furthermore, the relationship to a Fokker-Planck equation is facilitated in this representation. This brings up the problem of quantum action-angle coordinates.[21–24] Berman and Kolovsky have suggested an approach which may be useful for quantal studies like the present one.[24] There still remains the problem of proper coherent states for action-angle variables.[23] Work in the area of quantal analogs of action-angle variables is therefore extremely important and essential to the mapping of nonlinear classical dynamics to quantum theory.

We also attempted to obtain an analytic Fokker-Planck approximation to the evolution of the Wigner equation and it appears that it is not possible to achieve such an approximation. Deriving this quantal Fokker-Planck equation is important due to the fact that it provides a basis for a diffusive picture. Wigner in his 1932 paper[4] gives two forms of the evolution equation. The derivation of the first form assumes that the potential can be expanded in a power series. The singular nature of the Coulomb potential does not allow the use of the first form as a starting place. Further, the derivation of a Fokker-Planck equation requires the use of a power-series expansion. In performing this expansion even the second form fails to avoid the Coulomb singularity. It would appear that any evolution equation involving the SSE Wigner function (at least in Cartesian coordinates) will not circumvent this problem. In classical dynamics, the

Fokker-Planck equation is derived in action-angle coordinates which regularize the Coulomb singularity. However, it would be interesting to consider deriving the quantal Fokker-Planck equation for a Hamiltonian with a nonsingular potential. Work we have done to this point suggests that this is possible.

ACKNOWLEDGMENTS

This work has been supported by a grant from the National Science Foundation. Some of the numerical calculations were performed on the Cray-XMP at the Pittsburgh Supercomputing Center. The authors are grateful to L. Armstrong, Jr., for his comments.

[1]K. A. H. van Leeuwen, G. v. Oppen, S. Renwick, J. B. Bowlin, P. M. Koch, R. V. Jensen, O. Rath, D. Richards, and J. G. Leopold, Phys. Rev. Lett. **55**, 2231 (1985).

[2]J. E. Bayfield, Comments At. Mol. Phys. **20**, 245 (1987).

[3]R. V. Jensen, Phys. Rev. A **30**, 386 (1984); J. G. Leopold and D. Richards, J. Phys. B **1**, 1125 (1986).

[4]E. Wigner, Phys. Rev. **40**, 749 (1932); S. R. deGroot and L. G. Suttorp, *Foundations of Electrodynamics* (North-Holland, Amsterdam, 1972), Chap. VI.

[5]M. V. Berry, Philos. Trans. R. Soc. A **287**, 237 (1977).

[6]John S. Hutchinson and Robert E. Wyatt, Chem. Phys. Lett. **72**, 378 (1980).

[7]Shau-Jin Chang and Kang-Jie Shi, Phys. Rev. A **34**, 7 (1986).

[8]*Physics of Phase Space*, edited by Y. S. Kim and W. W. Zachary (Springer-Verlag, Berlin, 1987).

[9]G. Casati, B. B. Chirikov, D. L. Shepelyansky, and I. Guarneri, Phys. Rep. **154**, 77 (1987).

[10]T. Geisel, G. Radons, and J. Rubner, Phys. Rev. Lett. **57**, 2883 (1986).

[11]I. S. Gradshteyn and I. M. Ryzhik, *Tables of Integrals, Series and Products* (Academic, New York, 1980).

[12]J. N. Bardsley, B. Sundaram, L. A. Pinnaduwage, and J. E. Bayfield, Phys. Rev. Lett. **56**, 1007 (1986).

[13]S. Graffi, T. Paul, and J. H. Silverstone, Phys. Rev. A **37**, 2214 (1988).

[14]J. E. Moyal, Proc. Cambridge Philos Soc. **45**, 99 (1949).

[15]R. V. Jensen (private communication).

[16]K. Husimi, Proc. Phys. Math. Soc. Jpn. **22**, 264 (1940).

[17]A. K. Rajagopal, Phys. Rev. A **27**, 558 (1983).

[18]D. L. Shepelyanski, in *Chaotic Behavior in Quantum Systems*, edited by G. Casati (Plenum, New York, 1985), pp. 187–204.

[19]J. G. Leopold and D. Richards, J. Phys. B **21**, 2179 (1988).

[20]R. S. MacKay and J. D. Meiss, Phys. Rev. A **37**, 4702 (1988).

[21]M. Moshinsky and T. H. Seligman, Ann. Phys. (N.Y.) **120**, 402 (1979).

[22]R. G. Newton, Ann. Phys. (N.Y.) **124**, 327 (1980).

[23]P. Carruthers and M. M. Nieto, Rev. Mod. Phys. **40**, 411 (1968).

[24]G. P. Berman and A. R. Kolovsky, Physica **D8**, 117 (1983).